# Journal Pre-proof

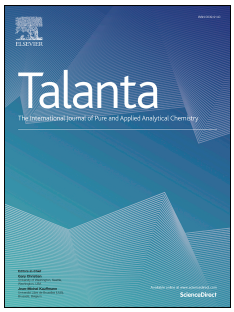


A high-sensitive electrochemical DNA biosensor based on a novel ZnAl/ layered double hydroxide modified cobalt ferrite-graphene oxide nanocomposite electrophoretically deposited onto FTO substrate for electroanalytical studies of etoposide

Fahimeh sadat Vajedi, Hossein Dehghani

PII: S0039-9140(19)31077-X

DOI: https://doi.org/10.1016/j.talanta.2019.120444

Reference: TAL 120444

To appear in: *Talanta*

Received Date: 16 August 2019

Revised Date: 25 September 2019

Accepted Date: 4 October 2019

Please cite this article as: F.s. Vajedi, H. Dehghani, A high-sensitive electrochemical DNA biosensor based on a novel ZnAl/layered double hydroxide modified cobalt ferrite-graphene oxide nanocomposite electrophoretically deposited onto FTO substrate for electroanalytical studies of etoposide, *Talanta* (2019), doi: https://doi.org/10.1016/j.talanta.2019.120444.

## Graphical abstract

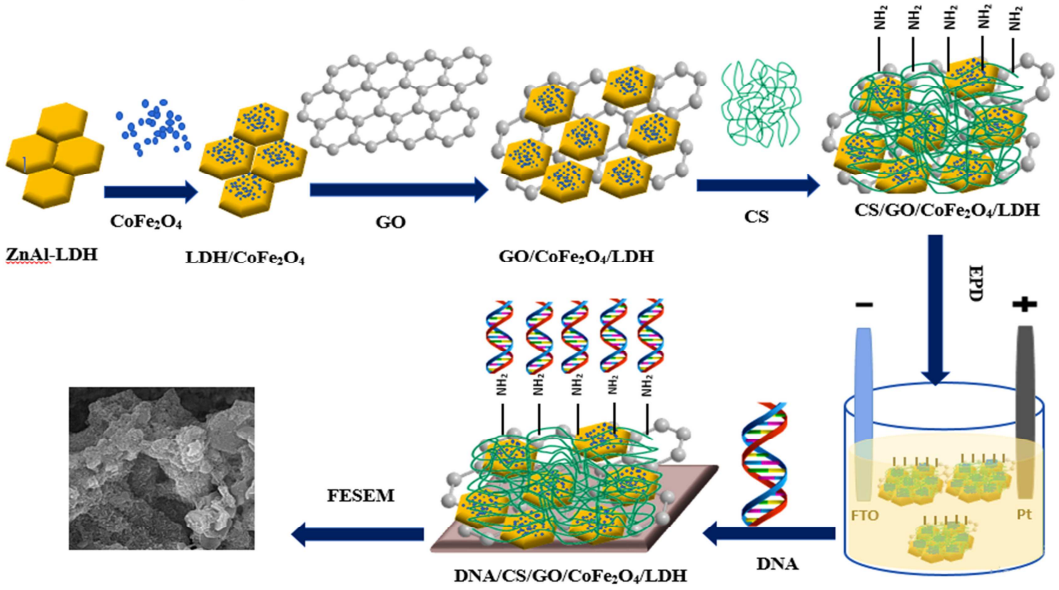

# A high-sensitive electrochemical DNA biosensor based on a novel ZnAl/layered double hydroxide modified cobalt ferrite-graphene oxide nanocomposite electrophoretically deposited onto FTO substrate for electroanalytical studies of etoposide

Fahimeh sadat Vajedi,[a] Hossein Dehghani [a] *

[a]Department of Inorganic Chemistry, Faculty of Chemistry, University of Kashan, P.O. Box 87317-51167, Kashan, Iran
Email: dehghani@kashanu.ac.ir
*Corresponding author, Tel: +98 315 591 2386. Fax: +98 315 591 2397, Iran, Area cod Box 87317-51167.

**Abstract:** The combination of layered double hydroxides (LDHs), cobalt ferrite ($CoFe_2O_4$) and graphene oxide (GO) creates a ternary nanocomposite that can incredibly improve advantages of each compound; this is an impressive way to attain multifunctional materials with attractive properties. In this study, a new high-sensitive electrochemical DNA biosensor was fabricated for the electroanalytical studies of etoposide using a novel ZnAl/layered double hydroxide modified cobalt ferrite- graphene oxide nanocomposite ($GO/CoFe_2O_4$/ZnAl-LDH) that was electrophoretically deposited (EPD) on the fluorine tin oxide (FTO) substrate. This DNA biosensor was prepared via electrostatic adsorption of DNA onto the $GO/CoFe_2O_4$/ZnAl-LDH/FTO electrode. The electrochemical behavior of electrodes was characterized using cyclic voltammetry (CV) and electrochemical impedance spectroscopy (EIS). EIS plot obviously demonstrated a rapid electron transport at low frequencies for $GO/CoFe_2O_4$/ZnAl-LDH. Differential pulse voltammetry (DPV) and square wave anodic stripping voltammetry (SWASV) were employed for the electrochemical detection of ETO. The results revealed that DNA/$GO/CoFe_2O_4$/ZnAl-LDH/FTO bioelectrode had ultrahigh sensitivity to ETO with the detection limit of 0.0010 µM in the linear range of 0.2-10 µM. In addition, the developed biosensor revealed precise reproducibility and excellent stability of about 95% of the initial activity after 6-7 weeks. On the other hand, the present bioelectrode was also capable of discriminating different interferences and was also used to detect etoposide in real samples such as human blood plasma, serum and urine with good recoveries, ranging from 97.0% to 104.0%. The obtained results of the excellent performance of this biosensor could be assigned to the active reaction sites and good electrochemical activity of nanocomposites, hence helping increase the DNA immobilization and accelerate the electron transfer more effectively on the surface electrode.

**Keywords**: DNA biosensor, Etoposide, Electrophoretic deposition, Ternary nanocomposite

## 1. Introduction

Etoposide (ETO) or VP-16 has been regarded as the substantial class of a potent clinical anticancer agent against various neoplastic diseases. ETO is a semi-synthetic podophyllotoxin derivative that due to its high potential can be deliverable by various nanomaterials.[1] It is extensively utilized for the treatment of different types of cancers, such as small lung cancers, lymphoma and leukemia that lead to DNA damage in cancer cells.[2] Currently, the precise mechanism of the drugs against cancer is still unknown, but ETO as a cell cycle-specific drug acts either by the formation of free radicals or by inhibiting the DNA-topoisomerases II which leads to DNA strand breakage and damaging the DNA of cancer cells.[3] However, the development of sensitive and accurate techniques for the testing and monitoring the drug levels in the biological samples is extremely desirable. A wide range of qualitative and quantitative methods has been applied to determine ETO including high performance liquid chromatography (HPLC),[4, 5] spectrofluorimetry[6] and liquid chromatography–mass spectrometry.[7] Current methods due to their use of expensive devices and solvents, are time consuming and offer a high detection limit for ETO. However, the electrochemical methods, due to their large variety of electrodes could be regarded as a promising alternative method showing rapid and sensitive detection, and offer more information about the electron transfer processes of ETO with lower costs.

Molecular bioelectronics have acquired wide attention due to their inherent specificity and sensitivity, good selectivity and strong operability.[8, 9] Since DNA plays an important role in cellular processes including copying, storage and transmission of gene messages, a lot of research has been conducted on the binding nature and dynamics of small molecules (pollutants, drugs) upon DNA and further understanding of the action mechanisms of anticancer drugs for the design of specific DNA-targeted drugs[10] the reason is that the presence of such drugs and chemicals by influencing the expression of the gene could lead to diseases that are associated with changes in cell proliferation and differentiation. Generally, the interaction mechanism of drugs with DNA occurs through various ways including intercalation, external electrostatic binding to the negatively charged nucleic acid and non-covalent groove binding.[11, 12] Spectroscopic, molecular modeling, HPLC and electrochemical techniques have been exploited for the characterization of the drug–DNA interaction.[13-15] Recently, electrochemical techniques have been proposed for the identification of the interaction mechanisms between DNA and drugs. Among them for such detection, the electrochemical DNA biosensors based on the changes in redox signals of the compounds and the conversion of them into useful response signals, have been extensively applied.[16, 17]

These DNA biosensors provide fast response, and simple and cost-effective detection of small compounds at the site of interest.[18] The immobilization of DNA onto the electrochemical transducer surface (here the nanoparticles coated FTO electrode) is a crucial step for the construction of high-performance electrochemical DNA biosensors so that the stability, sensitivity and accuracy of the biosensor are the substantial links that can further ensure the interaction of the DNA and small molecules.[19] Besides, the immobilization of DNA directly onto the bare surfaces of nanomaterials might cause its denaturation and loss of bioactivity. Due to their favorable structural, catalytic, magnetic, and electronic properties, numerous matrixes, such as carbon nanotubes, graphite, carbon electrodes, nanomaterials, conducting/semi-conducting materials like gold, platinum,[20] biopolymers and metal oxide nanoparticles and their composites due to their favorable structural, , catalytic, magnetic and electronic properties[21] have been utilized for the modification of the electrode surface and the facilitation of the specific binding behavior using physical adsorption, covalent-binding,[22] electrostatic binding[23] cross-linking[24] and self-assembly.[25] In general, the DNA adsorption without a covalent linkage is reversible. Specially, metal oxide nanoparticles and carbon-based nanomaterials, are potential candidate materials for the further development of electrochemical biosensors due to their large specific surface-to-volume ratio, enhanced electron transfer, conductivity, quantum-confinement effects, ease of handling, retention of the bioactivity because of the biocompatibility of the nanoparticles and size compatibility with biological compounds (such as proteins and nucleic acids).[26, 27] Singh's group have reported an electrochemical DNA sensor based on chemically Chitosan–iron oxide for the Neisseria gonorrhoeae detection.[28] Radi reported the electrochemical behaviors of the anticancer drug etoposide and its interaction with DNA in the solution phase using a DNA modified screen-printed carbon electrode (SPCE) by differential pulse voltammetric with detection limit 0.005 µM.[29]

As hydrotalcite-like anionic clay, layered double hydroxides (LDHs) with the general formula of $[M^{II}_{1-x}M^{III}_{x}(OH)_2]^{x+}[(A^{n-1})_{x/n}]^{x-}.mH_2O$, have attracted much attention for their application in numerous fields including electrochemical sensors, optical materials, separation and biology, [30-32] due to their positively charged layers with counter anions in the interlayer spacing, electrochemically active sites, specific layered structure, effective thermal stability and ion-exchange properties. LDHs and their nanocomposites have been applied for improving the performance of biosensors. For instance, Li et al have reported an electrochemical biosensor based on Ni/Al layered double hydroxide on Ti substrate for detection of the $H_2O_2$.[33] Despite the aforementioned properties for the LDHs, the electron transfer has been profoundly constrained due to the relatively poor conductivity of LDHs, difficult separation from solution and the tendency to aggregate together in the solid state. In addition, the electrical conductivity of

the LDHs-based electrochemical sensors has also considerable importance to make a fast response and a highly active and stable electrochemical platform. To overcome these shortcomings and improve the detection limit, a combination of magnetic nanoparticles with LDHs has been suggested for developing electrode materials with the desired functionality. Zhang et al have first prepared a new magnetic nano-scale catalyst, including LDHs with magnesium ferrite.[34] Among various metal oxide nanoparticles, ferrites especially the $CoFe_2O_4$ nanoparticles (NPs) with cubic spinel structure have been identified as potential candidate materials to promote faster electron transfer kinetics. $CoFe_2O_4$ exhibits a large surface-to-volume ratio, different redox states, convenient control over the electrode, excellent electrochemical stability, high conductivity and strong adsorption ability.[35] These nanoparticles have unique applications in the immobilization of biomolecules, biosensors, solar cells, drug delivery and the removal and detection of heavy metal ions. [36-38] However, one of the key problems for the preparation of fairly uniform $CoFe_2O_4$ NPs is the agglomeration of the magnetic nanoparticles due to the magnetic dipole interaction between nanoparticles and the high surface area that limits the practical applications of the above-mentioned properties. On the other hand, the incorporation of graphene oxide nanosheets with metal oxide nanoparticles is greatly desirable to overcome these problems and achieve increased sensing properties. Shahnavaz et al[39] fabricated a reduced graphene oxide-supported copper ferrite hybrid and found this composite demonstrating the highest glucose oxidation current compared to the pure $CoFe_2O_4$. As an emerging form of carbon materials, graphene oxide (GO) or reduced graphene oxide (RGO) is a single layer of $sp^2$-bonded carbon atoms with such unique properties, as high surface area, excellent electrical conductivity and potential low manufacturing cost.[40] These properties, along with abundant functional groups such as hydroxyl and epoxide groups on the basal planes and carbonyl groups at the edges of the sheet, make GO (or RGO) suitable for a wide range of applications, including biosensors, targeted drug delivery and the removal of organic pollutants.[41, 42] The presence of $CoFe_2O_4$/LDH on electrode surface provides an improved electrochemical response due to the unique characteristics of $CoFe_2O_4$/LDH such as good electrical conductivity, electroactive surface area and high chemical stability. These properties of $CoFe_2O_4$/LDH together with the GO promote charge transfer reactions. In view of what was said, the construction of the GO/$CoFe_2O_4$/LDH composites for an electrochemical sensor is a great choice. Wu et al and Zhang et al fabricated magnetite− GO−LDH composites for the removal of Pb (II) and an organic pesticide from aqueous solutions.[43, 44]

Nowadays, the study of nanomaterial-based composites for the fabrication of the electrochemical DNA biosensor for the sensitive detection of drugs is still in the early stages. On the other hand, electrochemical methods have received much attention as a suitable detection tool for rapid investigation in the

field of biosensors. In previous electrochemical studies, the ETO detection was performed using carbon-based nanostructures at GCE, $SiO_2$ and SPCE electrodes[29, 45, 46] with limit detection (0.005, 005, 0.004 µM, respectively), to the best of our knowledge, there are no previous reports available on the preparation of the electrochemical DNA biosensors based on nanostructures for the detection of drugs, especially ETO. This study, for the first time, reports on a new strategy for the fabrication of the electrochemical DNA biosensors in the detection of drugs, along with the integration of ZnAl-LDH nanosheets, $CoFe_2O_4$ nanoparticles and GO to form a novel nanocomposite material deposited on fluorine tin Oxide (FTO) substrates by the electrophoretic deposition (EPD) technique. The EPD technique is known as a simple, rapid and cost-effective method for the preparation of thin films of nanomaterials and nanocomposites on conductive substrates that can produce uniform and stable layers of controlled thickness compared to other coating techniques.[47] Additionally, this technique is especially suitable to investigate the charge transfer properties and ion exchange at the electrode-electrolyte interface. FTO sheets can be used as an appropriate substrate owing to their high electrical conductivity, excellent chemical stability and visible transparency. Furthermore, FTO glass sheets are cheap because of the natural abundance of fluorine compared to indium element and have good thermal stability and diffusion compared to indium tin oxide (ITO). The purpose of this study was, thus, to address the critical aspects of treatment such as improved sensitivity and detection limit below the therapeutic concentration range using the DNA/GO/$CoFe_2O_4$/ZnAl-LDH/FTO bioelectrode.

## 2. Experimental

### 2.1 Materials and Chemicals

Salmon sperm DNA sodium salt was purchased from the Serva Company (India). Etoposide in its pharmaceutical dosage form was kindly provided by EBEWE Pharmaceutical Company (AUSTRIA). A stock solution of DNA was prepared in Tris–EDTA buffer (TE, 0.1 M Tris HCl, 0.05 M EDTA) of pH 8.0 and stored at 4 °C prior to use. The molar concentration of DNA was determined by UV according to the absorbance at 260 nm.[48] Chitosan (CS) was purchased from Sigma. All other chemicals used in this study for the preparation of nanomaterials and supporting electrolytes were of analytical reagent grade (Merck or Sigma) and used as received without further purification. Double distilled water and ethanol were used as solvents. A 20 mM phosphate buffer solution (PBS) with a pH range of 7.0–7.5 was applied as a supporting electrolyte for the electrochemical measurements using $Na_2HPO_4$ and $NaH_2PO_4$ salts. The diluted solutions of DNA and drug were obtained indirectly with TE and phosphate

buffer solutions, respectively. The fluorine-doped tin oxide (FTO) glass substrates (transmission >90% in the visible, sheet resistance 8 Ω per square and 2.3 mm thickness) were obtained from Dyesol (Australia).

### 2.2 Apparatus

The structural characteristics of the prepared materials were characterized by a powder X-ray diffractometer on Phillips X'Pert PRO with a Cu Ka radiation (λ=1.541 □) in the range of 0˚- 80˚ Bragg's angle. The average nanocrystalline sizes, D, were evaluated by the Scherrer's formula, $D = 0.89\ \lambda / \beta \cos\theta$, where λ is the wavelength of the X-rays, β is the FWHM and θ is the Bragg diffraction angle. The fourier transform infrared (FT-IR) spectroscopy measurements were performed using a Magna 550 Nicolet instrument on pressed KBr pellets to characterize the bonds forming and skeletal vibration of the samples in the nanostructures in the wavenumber range of 400 to 4000 $cm^{-1}$. The study on the general morphology and elemental composition of the GO/$CoFe_2O_4$/LDH/FTO electrodes and the dsCT-DNA /GO/$CoFe_2O_4$/LDH-modified bioelectrodes were carried out using field emission scanning electron microscopy and Energy-dispersive X-ray spectroscopy (EDX) instrument (TESCAN BRNO-Mira3 LMU). In addition, tapping mode atomic force microscopy (AFM) (Shimadzu Corporation, Japan) was applied to characterize the surface roughness of the samples. All electrochemical measurements such as cyclic voltammetry (CV), square wave anodic stripping voltammetry (SWASV) and differential pulse voltammetry (DPV) (Sama 500 potentiostat (Isfahan, Iran) and electrochemical impedance spectroscopy (EIS, AUTOLAB Potentiostat Galvanostats) were performed with a conventional three-electrode system consisted of a FTO (working), platinum wire (counter) and Ag/AgCl (reference) electrodes in phosphate buffer (PBS, 20 mM, pH 7.4, 0.9% NaCl) containing 5 mM $[Fe(CN)_6]^{3-/4-}$.

### 2.3 Synthesis of Zn-Al LDH nanosheets

The Zn/Al-LDHs nanosheets with a Zn/Al molar ratio of 2 were synthesized via a hydrothermal method. In brief, an aqueous solution containing ZnCl2.6$H_2O$ (10 mM), $AlCl_3 \cdot 6H_2O$ (5 mM) and hexamethyl-enetetramine (HMT) at 30 mM concentration was vigorously stirred at room temperature for 30 min. The solution pH was regulated by HMT, through the hydrolyzation and release of ammonia at high tempera-ture. The suspension was transferred into an autoclave and heated at 100 °C for 48 h. The resulting precip-itate was thoroughly washed with Milli-Q water several times, centrifuged and finally dried at 60 °C over-night.

### 2.4 Synthesis of $CoFe_2O_4$ nanoparticles

The synthesis of the $CoFe_2O_4$ nanoparticles was carried out by a surfactant-assisted hydrothermal process. In a typical synthesis, the stoichiometric quantities of $Fe(NO_3)_3.9H_2O$, $Co(NO_3)_2.6H_2O$, polyethylene glycol (PEG-200) and oxalic acid (in molar ratios of 2:1:1:1) were dissolved thoroughly in the desired volume of distilled water under stirring for 30 min at room temperature to obtain a homogeneous dispersion. After continued stirring, the solution was transferred to an autoclave and treated at 150 °C for 20 h. The product was washed with deionized water and alcohol several times to remove the impurities and dried at 70 °C for 12 h. The precipitation of cobalt iron oxalate precursor was then annealed at 500 °C for 3 h.

### 2.5 Preparation of GO/$CoFe_2O_4$/Zn-Al LDH by the self-assembled process

GO was synthesized using a modified version of the Hummers method.[49] The GO/$CoFe_2O_4$/Zn-Al LDH nanocomposites were synthesized by alternately adsorption Zn-Al LDH with $CoFe_2O_4$ and GO in a mass ratio of 2:1:0.5, respectively. Briefly, a calculated amount of $CoFe_2O_4$ nanoparticles was added into an aqueous solution of Zn-Al LDH (50 ml, 1 mg/mL) by ultrasonication for 1 h. The resulting dispersion was rinsed with ultra-pure water. Then, the solution of GO (100 mL, 0.2 g/L) was added to the obtained $CoFe_2O_4$/Zn-Al LDH and the mixed system was ultrasonicated for 40 min. The black precipitate was collected and dried at 60 °C, yielding the GO/$CoFe_2O_4$/Zn-Al LDH.

Afterward, the GO/$CoFe_2O_4$/Zn-Al LDH composite was suspended in 10 ml of a 0.2 mg $mL^{-1}$ solution of CS (20 mg of chitosan in 100 ml of acetate buffer 0.05 M, pH 4.2) stirred for 30 min followed by sonication at room temperature for about 1 h to get a uniformly dispersed mixture.

### 2.6 Electrophoretic deposition of GO/$CoFe_2O_4$/Zn-Al LDH onto FTO electrode

All the nanocomposite films were fabricated on the conducting substrates (FTO) using the electrophoretic deposition technique (EPD). Prior to the fabrication of the multilayered films, FTO glass substrates (1.5cm×1.5 cm, diameter=2mm) were precleaned ultrasonically in acetone, ethanol and deionized (DI) water for 15 min each and dried at 450 °C. The hydrophilic and negatively charged surface of FTO was obtained after immersing in a fresh solution of $H_2O_2/NH_4OH/H_2O$ (1:1:5, v/v) at 90 °C. The FTO substrates were chosen because the bearing an oxide surface. For the EPD of the nanocomposites, the prepared nanocomposites were dispersed in ethanol solvent (1: 3 ratio) after 1 h sonication. During the EPD process, the migration of nanocomposites colloids toward cathode demonstrates that these have a

positive charge in the solution due to the presence of $NH_3^+$ in chitosan on the surface of the nanocomposites. The FTO electrode with a positive potential (anode) and a platinum electrode as the counter-electrode (cathode) were placed vertically and immersed into the suspension solution of the nanocomposites in the EPD cell by separation 1 cm. The EPD technique was performed at a constant potential for about 30 min on the FTO glasses after the optimization of the applied voltage (2−20 V) and deposition time (60 s- 1h). Then, the prepared electrodes were washed with deionized (DI) water to remove excess or unbound particles, air-dried and kept in desiccated condition for further use. The modified electrode was denoted as the GO/$CoFe_2O_4$/LDH/FTO. As a comparison, the LDH/FTO and $CoFe_2O_4$/LDH/FTO electrodes were prepared under the same conditions.

### 2.7 Fabrication of DNA/GO/$CoFe_2O_4$/LDH/FTO bioelectrode

Adsorption immobilization of DNA was performed by dropping 10.0 μL of the fresh solution of DNA in Tris- EDTA (TE) buffer (pH 8.0) directly onto the GO/$CoFe_2O_4$/LDH/FTO electrode followed by 2 h incubation at 25 °C. The negatively charged DNA molecules interacted electrostatically with the positively charged CS modified nano GO/$CoFe_2O_4$/LDH/FTO electrode due to the presence of phosphate groups ($PO_4^-$) on its backbone. This bioelectrode was subsequently rinsed with TE buffer to remove any unbound DNA on the surface of the electrode and stored at 4 °C to further use. The different steps for the fabrication of DNA biosensor are shown in Scheme 1.

## 3. Results and discussion

### 3.1. Characteristics of the modified electrode

The successful preparation of the GO/$CoFe_2O_4$/LDH/FTO electrode for the ETO detection is an important principle through the whole system. Firstly, the prepared GO/$CoFe_2O_4$/LDH/FTO electrode was characterized by AFM. Fig. 1 depicts the 3D AFM images of an electrochemically deposited the GO/$CoFe_2O_4$/LDH/FTO electrode (a) and DNA/GO/$CoFe_2O_4$/LDH/FTO bioelectrode (b) scanned at a rate of 1 Hz. The AFM studies have indicated that the root-mean-square (RMS) roughness values of GO/$CoFe_2O_4$/LDH/FTO and the DNA/GO/$CoFe_2O_4$/LDH/FTO are estimated to be about 58 nm and 30 nm, respectively, showing that the electrode before the immobilization of DNA has much rougher surface compared with that after the immobilization of DNA with the smoother surface. These results clearly indicate that the DNA molecules were well immobilized on the surface electrode.

The surface morphology of the GO/$CoFe_2O_4$/LDH/FTO electrode before and after DNA immobilization was investigated by FE-SEM (Fig. 2). Fig. 2a reveals the morphology of the uncoated GO/$CoFe_2O_4$/LDH/FTO. It is apparently seen from Fig 2a that both the hexagonal crystals of LDH and the $CoFe_2O_4$ nanospheres uniformly agglomerated on the surface of GO, revealing the formation of the GO/$CoFe_2O_4$/LDH nanocomposite with rough porous morphology. Fig. 2b exhibits that the morphology of the GO/$CoFe_2O_4$/LDH nanocomposite was well preserved after the efficient coating of DNA. It is noticeable that a favorable environment is provided by the GO/$CoFe_2O_4$/LDH nanocomposite for DNA immobilization via electrostatic interactions between cationic CS surface and negative DNA molecules. Furthermore, this porous network provides an effective surface of the substrate electrode to immobilize large amounts of DNA and prevents DNA from leaching.[50] The EDX data of the GO/$CoFe_2O_4$/LDH/FTO nanocomposite in Fig. 2C shows the existence of the Zn, Al, Fe, Co, O, N and C elements, conforming the composition of LDH and $CoFe_2O_4$ on the GO surface. Whereas, after the immobilization of DNA (Fig. 2d), the presence of an additional peak of phosphorus (P) gives the evidence that DNA was well immobilized on the surface of electrode.

The XRD patterns of the pristine ZnAl-LDH, $CoFe_2O_4$, $CoFe_2O_4$/ZnAl-LDH and GO/$CoFe_2O_4$/ZnAl-LDH are shown in Fig. 3. The diffraction peaks of the Zn-Al LDH/$CoFe_2O_4$ at 2θ= 30.48˚ (220), 35.86˚ (311), 37.13˚ (222), 43.5˚ (400), 53.96˚ (422), 57.46˚ (511), 62.97˚ (440) and 74.91˚ (533) can be indexed to a typical cubic (fcc) crystal structure model (JCPDS No.22-1086) of the $CoFe_2O_4$ nanoparticles, while 2θ= 11.55˚, 23.14˚, 34.64˚, 39.19˚, 46.63˚, 52.65˚, 55.93˚, 60.22˚ and 61.53˚ correspond to the (003), (006), (012), (015), (018), (1010), (0111), (110), and (113) planes of Zn/Al LDH nanosheets, respectively (JCPDS file No. 38-0486). The main peaks of LDHs and $CoFe_2O_4$ are well maintained with those of LDH/$CoFe_2O_4$. It has to be noted that, no significant differences can be observed in the XRD pattern for the GO/$CoFe_2O_4$/ZnAl-LDH nanocomposites after the addition of GO, which may be due to their low content in the composites, Low intensity diffraction, fine dispersion of GO in the composites and/or the overlaps with the (006) strong peak of the Zn-Al LDH at 23.14°. The observation of the XRD results confirms the successful preparation of the GO/$CoFe_2O_4$/ZnAl-LDH nanocomposites.

The formation of the LDH, $CoFe_2O_4$, $CoFe_2O_4$/ZnAl-LDH and GO/$CoFe_2O_4$/ZnAl-LDH nanocomposites were further investigated by FTIR spectroscopy in the range 400− 4000 $cm^{-1}$ (Fig. 4). In the spectrum of $CoFe_2O_4$, the absorption bands observed at 3430 and 1626 $cm^{-1}$ are related to the O–H stretching vibration and bending vibration of the adsorbed water molecules on the surface of the ferrite nanoparticles, and the higher frequency band ($\upsilon_1$) (570 $cm^{-1}$) and the lower frequency band ($\upsilon_2$) (430 $cm^{-1}$) correspond to the stretching vibrations of the tetrahedral groups ([$Co^{2+}$- $O^{2-}$] and [$Fe^{3+}$-$O^{2-}$]) and the

stretching vibrations of [$Fe^{3+}$- $O^{2-}$] at the octahedral sites of the spinel structure, respectively.[51] In the spectrum of LDH, two common bands at 3433 and 1623 $cm^{-1}$ are also detected, which could be attributed to the hydrogen-bonded to metal-OH groups in the brucite layers and in the interlayer water molecules and the water deformation band. The bands appeared from ~1000 to 400 $cm^{-1}$ in the low wavenumber region can be attributed to the metal-oxygen lattice vibrations like Zn–O and Al–O in the octahedral hydroxyl sheets. Furthermore, the characteristic bands at around 1390 and 880 $cm^{-1}$ are assigned to the $\nu_3$ and $\nu_2$ modes of interlayer $CO_3^{2-}$ ions, respectively. [44] The FT-IR spectrum of the $CoFe_2O_4$/ZnAl-LDH sample revealed a combination of the spectral band features of pure $CoFe_2O_4$ and pristine ZnAl-LDH, although some vibrations overlapped. Hence, the gained results proved the formation of the $CoFe_2O_4$/ZnAl-LDH nanocomposites. In the spectrum of GO, the peak at 1728 $cm^{-1}$ can be corresponded to the C=O stretching vibrations of the carboxylic acid (-COOH) groups or carbonyl moieties, while the intense peaks at 3407 and 1619 $cm^{-1}$ can be ascribed to the stretching vibrations of the -OH band and C=C deformation vibration, respectively. The peaks at 1385 and 2926-2853 $cm^{-1}$ belong to the C-OH stretching vibration of the carboxylic acid groups and the symmetrical and asymmetrical stretching vibrations mode of C-H aromatic. The peaks at 1229 and 1070 $cm^{-1}$ are attributed to the stretching vibration band of alkoxy (C–O). In addition, the bands position shifted after the interaction of the $CoFe_2O_4$/ZnAl-LDH nanocomposites with GO to a lower wavenumber due to the covalent linkage of nanocomposites onto the GO surface.

### 3.2 Electrochemical behavior of modified electrodes

The electrochemical behavior of the different modified electrodes was also investigated using Cyclic Voltammetric (CV) and Electrochemical Impedance Spectroscopy (EIS) in PBS (20 mM, pH 7.4, 0.9% NaCl) containing $[Fe(CN)6]^{3-/4-}$ (5 mM)] (Fig. 5).

Fig. 5 shows the typical CV sweep curve obtained for bare the FTO, LDH/FTO, $CoFe_2O_4$/LDH/FTO, GO/$CoFe_2O_4$/LDH/FTO and DNA /GO/$CoFe_2O_4$/LDH/FTO bioelectrode, respectively, to investigate the changes of the redox behavior of modified electrodes after each assembly step at a scan rate of 100 mV/s. From the CV curve results, a pair of well-defined reversible redox peaks for all the prepared electrodes is clearly evident, suggesting a quasi-reversible electrode process. The CV of bare the FTO shows a couple of redox peaks corresponding to the electron transfer of $[Fe(CN)_6]^{3-}$/$[Fe(CN)_6]^{4-}$ with the anodic (Epa) and cathodic (Epc) peak potential of 0.148 V and -0.157 V, respectively having peak oxidation current (Ipa) about 1117 μA. After the deposition of LDH nanosheets onto FTO, the peak current increases significantly to 1629 μA while a negligible change is observed in the peak to the peak separa-

tion potential (0.017 V) compared to bare the FTO electrode, indicating a highly improved redox behavior of the LDH/FTO electrode that may be attributed to the electrostatic attraction of the electroactive ferro and ferricyanide ions to the LDH cationic nanosheets. Furthermore, a larger surface area is provided for the diffusion of $[Fe(CN)_6]^{3-/4-}$ towards the electrode surface. The peak current of the $CoFe_2O_4$/LDH /FTO (2062 µA) is higher with the peak-to-peak separation voltage of 0.04 V in comparison to with that LDH/FTO, which is due to the good electron communication properties of $CoFe_2O_4$ and the improvement in the electrical conductivity and electron transfer between the electrode and the electrolyte. The magnitude of peak current (3921 µA) and peak-to-peak separation potential (0.074 V) increases considerably after the integration of GO onto the $CoFe_2O_4$/LDH /ITO electrode surface. This improved electrochemical behavior of the electrode can be due to the high conductivity, unique electronic structure of GO and high surface area that facilitating their electron transfer at electrode. [52] Finally, the further decrease in the peak oxidation current to 3537µA along with a decrease in the peak-to-peak separation of the redox potential (0.04V) were observed after immobilizing DNA onto the GO/$CoFe_2O_4$/LDH/FTO electrode via electrostatic interactions between cationic chitosan matrix and polyanionic phosphodiester backbones of DNA. This decrease of peak current can be probably attributed to the repulsive forces between the negatively charged phosphate backbone of DNA present onto the GO/$CoFe_2O_4$/LDH/FTO electrode surface and the negative charged $[Fe(CN)_6]^{3-/4-}$, indicating slower electron transfer kinetics because of the long polymer chain of DNA and resulting in reduction peak current. The result indicated that DNA had been successfully immobilized onto the electrode surface.

### 3.3 Effect of scan rate

Fig. 6a exhibits the effect of scan rates (υ, 10-400 mV $s^{-1}$) on the peak current to study the various kinetic parameters of the GO/$CoFe_2O_4$/LDH/FTO electrode and DNA/GO/$CoFe_2O_4$/LDH/FTO bioelectrode in PBS 20 mM. As evident, a significant rise is observed in redox the peak currents (Ipa & Ipc) linearly with a square root of scan rate ($\upsilon^{1/2}$) for both the electrodes (Fig. 6a and b; inset i), suggesting a diffusion-controlled electron-transfer process at the modified electrode that follows the equation: [53] (1) - (4)

$I_{pa}$ (GO/$CoFe_2O_4$/LDH/FTO) = 272.45 [µA] + 94.688 µA (s/mV) [scan rate (mV/s)] (1)
$R^2$ = 0.9971

$I_{pc}$ (GO/$CoFe_2O_4$/LDH/FTO) = −162.13 [µA] -210.33µA (s/mV) [scan rate (mV/s)] (2)
$R^2$ = 0.9948

$I_{pa}$ (dsCT-DNA /GO/$CoFe_2O_4$/LDH/FTO) = 256.71 [µA] + 418.28 µA (s/mV) [scan rate (mV/s)] (3)
$R^2$= 0.9971

$I_{pc}$ (dsCT-DNA /GO/$CoFe_2O_4$/LDH/FTO) = −235.22 [µA] – 441.74 µA (s/mV) [scan rate (mV/s)] (4)
$R^2$ = 0.9967

**3.4 Electrochemical impedance studies**

The effect of the changes occurring during the surface modification process on the interfacial electron-transfer resistance ($R_{et}$) was also characterized by electrochemical impedance spectroscopy (EIS). Fig. 7 displays the results of the EIS measurements obtained for the various electrodes in the PBS solution (pH 7.4) containing 5 mM $[Fe(CN)_6]^{3-/4-}$ as the redox probe in the constant frequency range of 100 kHz to 0.01 Hz at 0.25 V .In EIS, the semicircle portion observed at the higher frequencies region attributes to the charge transfer-controlled process, while a straight sloping line seen at lower frequencies corresponds to the diffusion-controlled process. As shown in Fig. 7 (inset), the Randles equivalent circuit was utilized for modelling the data obtained from the EIS measurements, which contains solution resistance ($R_s$), charge transfer resistance ($R_{ct}$) and the Warburg impedance ($Z_w$) resulting from the ions diffusion resistance of the redox probe in the electrodes structure. A parallel combination of the two elements of the Randles equivalent circuit, $R_{ct}$ and double layer capacitor ($C_{dl}$) represent the dielectric and insulating nature at the electrode/electrolyte interface. Among these aforementioned parameters, the recorded $R_{ct}$ value we utilized after each modification step, because the electrode modification processes strongly affect the electron transfer kinetic at the electrode interface and the redox probe.

The EIS plot indicated that the $R_{ct}$ of the bare FTO, LDH/FTO, $CoFe_2O_4$/LDH/FTO and GO/$CoFe_2O_4$/LDH/FTO were 75.3, 66.4, 57.1 and 26.5 Ω, respectively. It is clearly observed that the charge-transfer resistance value for bare the FTO is significantly largest of all suggesting a diffusion limited electrochemical process on this electrode. Furthermore, the values of the $R_{ct}$ for different electrodes deteriorate progressively in the order of LDH/FTO > $CoFe_2O_4$/LDH/FTO > GO/$CoFe_2O_4$/LDH/FTO. This indicates that the low $R_{ct}$ value for the LDH /FTO, as compared to that for the bare FTO might have occurred due to the ion-exchange and layered structure characteristics and electrostatic interactions between positive charged layers of LDH and the negatively charged $[Fe(CN)_6]^{3-/4-}$ probe. As a result, the accumulate of more ions ($Fe^{+2}/Fe^{+3}$) and effective surface of electrode can increase due to the presence of LDH which leads to poor LDH/FTO conductivity. Furthermore, this decreasing trend of the $R_{ct}$ in the $CoFe_2O_4$/LDH/FTO and GO/$CoFe_2O_4$/LDH/FTO electrodes

reveals that the presence of $CoFe_2O_4$ nanoparticles or GO on the electrode surface provides an increased electroactive surface, thus leading to more electrons transfer to electrode from the redox probe, and suggesting that GO has good electrical conductivity that facilitates electron transfer more effectively on the surface electrode and improves the electrochemical behavior of the electrode towards the redox probe. The obtained results reveal that the best electrochemical behavior among all of the electrodes observes for the GO/$CoFe_2O_4$/LDH/FTO electrode. The results of impedance experiments were congruous with the CV results. Upon the immobilization of DNA over GO/$CoFe_2O_4$/LDH/FTO electrode, there was a significant increase in the $R_{ct}$ value than that for the GO/$CoFe_2O_4$/LDH/FTO electrode because of more electrostatic repulsive force between the electro-negative phosphate group in DNA and the negatively charged redox species preventing the movement of $[Fe(CN)_6]^{3-/4-}$ ions towards the electrode during redox reaction. This also confirms that DNA is successfully immobilized onto the prepared GO/$CoFe_2O_4$/LDH/FTO electrode surface.

### 3.5 Electrochemical response studies of DNA/GO/$CoFe_2O_4$/LDH/FTO bioelectrode

In order to investigate the electrochemical properties of the modified electrodes differential pulse voltammetric (DPV) and square wave anodic stripping voltammetry (SWASV) were performed and recorded. Fig. 8a, b and c display DPV and square wave anodic stripping voltammetry (SWASV) response of bare the FTO (Curve a), LDH/FTO (Curve b), $CoFe_2O_4$/LDH/FTO (Curve c), GO/$CoFe_2O_4$/LDH/FTO (Curve d) and DNA /GO/$CoFe_2O_4$/LDH/FTO bioelectrode (Curve e), respectively in the absence and the presence of the ETO in PBS solution containing 5mM$[Fe(CN)_6]^{3-/4-}$ as the background electrolyte. The DPV parameters were carried out for the potential range of 0 V to 0.5 V using a pulse amplitude 50 mV, pulse width 30 s, sample width 0.02 s. It is evident that, the LDH/FTO electrode (curve b) shows an increase in peak current as compared to that of the bare FTO (curve a). The value of response current (1058 µA) in case of $CoFe_2O_4$/LDH/FTO (curve c) has increased suggesting the strong electrical conductivity of $CoFe_2O_4$. A sharp increase in the magnitude of the peak current (1402.8 µA) (curve e) is observed after the integration of GO onto the $CoFe_2O_4$/LDH /ITO electrode surface, which is due to the presence of extra non-binding sites on GO, good electrical conductivity resulting in faster electron transfer and increased electroactive surface area. Interestingly, the magnitude of the maximum current decreases to 1278 µA (curve d) with the immobilization of DNA on the GO/$CoFe_2O_4$/LDH/FTO electrode surface via electrostatic interactions between the positive charged cationic chitosan and polyanionic phosphodiester backbones of DNA, which might be due to the immobilization of DNA onto the surface of electrode leading to blocking the electron transfer between the electrode and the redox probes in the

solution. The obtained sensing results for the electrodes by SWASV illustrate that the response of each electrode to the ETO in the absence and the presence 5mM$[Fe(CN)_6]^{3-/4-}$ (Fig. 8b and c) is the same as the increase in the current of the electrodes measured by DPV in the absence of ETO. However, the obtained peak currents at the electrodes increase and the position of the potential peak measured by CV (0.1 V) shifts to the negative potential (from 0.1v to -0.48, Fig. 8b and from 0.1v to -0.15, Fig. 8c). The results show that these changes might be due to the effect of both intercalation and electrostatic interactions of ETO with the electrodes and good sensitivity of the electrodes at the ETO determination. The observed electrochemical behavior for DPV and SWASV is in agreement with the results in CV.

The electrochemical response of the DNA /GO/$CoFe_2O_4$/LDH/FTO bioelectrode as a function of ETO concentration varying from 0.2–10 µM was measured using DPV in phosphate buffer (20 mM, pH 7.4) containing 5 mM $[Fe(CN)_6]^{3-/4-}$ (Fig. 9). It was observed that the magnitude of the current response obtained for the DNA/GO/$CoFe_2O_4$/LDH/FTO bioelectrode at a potential of -0.1 V decreased proportionally as the ETO concentration increased. The observed decrease in the peak current could be assigned to the strong interaction of the drug with the surface-confined DNA layer. The results might have occurred due to the effect of both intercalation and electrostatic interactions of ETO with the anionic phosphate moieties of DNA. As seen in the inset of Fig. 9, there is a linear relationship between the peak current and ETO concentrations according to the following equation: $i_{pa}(\mu A) = 1054.2\text{-}63.408\ C\ (\mu M)$, with a standard deviation (SD) of 3.7 % and correlation coefficient of 0.9927. The detection limit (LOD) is calculated from the equation of 3SD/m, where SD and m are the standard deviation of the blank and the slope of the calibration curve, respectively, was found to be 0.0010 µM. The DNA /GO/$CoFe_2O_4$/LDH/FTO bioelectrode displayed a low detection limit with the high sensitivity of 63.408 µA/µM compared with those for the FTO, LDH/FTO, $CoFe_2O_4$/LDH/FTO and GO/$CoFe_2O_4$/LDH/FTO (data not shown). As demonstrated above, the fabricated DNA /GO/$CoFe_2O_4$/LDH/FTO bioelectrode exhibited the improvement in the detection limit compared to the other electrodes given in Table 1. This might be attributed to the excellent electrical conductivity, high surface of the fabricated matrix to the DNA immobilization and good electron communication obtained by the prepared nanocomposite.

**Table 1.** Comparison of the analytical parameters for etoposide detection using different electrode configurations

| Method | Electrode | Modifier | *Linear dynamic range (µM)* | *LOD (µM)* | *Ref.* |
|---|---|---|---|---|---|
| Electrochemistry | CPE | - | 0.25-25.0 | 0.10 | [3] |
| | GCE | - | 0.06-10 | 0.017 | [54] |
| | GCE | MWCNT | 0.02-2.0 | 0.005 | [47] |
| | SPCE | DNA | 0.1-10 | 0.005 | [29] |
| | GCE | CQDs | 0.02-10.0 | 0.005 | [54] |
| | $SiO_2$ | GNWs | 0.05-1 | 0.004 | [46] |
| | FTO | DNA/GO/$CoFe_2O_4$/LDH | 0.2-10 | 0.001 | This work |

CPE: Carbon paste electrode

GNWs: Graphene Nanowalls

SPCE: screen-printed carbon electrode

### 3.6 Reproducibility, Stability and Selectivity of the bioelectrode

The Reproducibility, operation stability and storage stability of the DNA/GO/$CoFe_2O_4$/LDH/FTO bioelectrode as two important factors for the determination of ETO were evaluated using DPV in optimized experimental conditions (Fig. 10).

The reproducibility of any biosensor is a measure of the results performed over a period of time. In this paper, the reproducibility of the DNA/GO/$CoFe_2O_4$/LDH/FTO bioelectrode was investigated using two measurements in the buffer solution (pH 7.4) containing the 10 µM ETO solution. The relative standard deviation (R.S.D.) of 3.55% was estimated in response to the 10 ETO µM ETO using five different electrodes, showing high reproducibility of the constructed DNA electrochemical biosensor. Additionally, the proposed bioelectrode could be regenerated and utilized for at least 9 times with a relative standard deviation of 5.2%. The stability analysis of the designed biosensor was determined by its shelf-life study.

To evaluate the operation stability, the DNA /GO/$CoFe_2O_4$/LDH/FTO bioelectrode was applied for sensing 10 μM ETO in the buffer solution (pH 7.4) for 30 CV cycles. Fig. 10a displays the 1st to 30st cycles in the electrochemical sensing of ETO. No significant changes in current response were observed as compared with the current response attained before storing as remained about 95% of its initial value even after 30 cycles. The results present the good operation stability of the sensor. The storage stability of the DNA /GO/$CoFe_2O_4$/LDH/FTO bioelectrode was tested by keeping the bioelectrode in a refrigerator (4 °C) at regular interval for about 1 week and the obtained peak currents of ETO were plotted in a bar chart. There were not significant changes in current response as compared with the current response attained before storing as remained about 95% of its initial value even after 6-7 weeks of storage (Fig. 10b). The high reproducibility and stability confirmed the suitability of the DNA /GO/$CoFe_2O_4$/LDH/FTO bioelectrode for the analysis of actual samples.

To determine the selectivity of the DNA /GO/$CoFe_2O_4$/LDH/FTO bioelectrode, the effect of some interfering agents existing in the biological samples (human blood/serum) was evaluated by the DPV method in the solution containing 10.0 μM of ETO as listed in Table 2. In this experiment, the change in the oxidation peak current response was studied in the absence and presence of such interfering species such as uric acid, glucose, ascorbic acid (AA), citric acid (UA), methionine, valine, caffeine, ibuprofen, acetaminophen and metal ions as $Na^+$, $K^+$, $Ca^{2+}$, $Mg^{2+}$, $Fe^{2+}$ at their physiological concentration. The results showed that the current response of ETO in the biological samples by the DNA /GO/$CoFe_2O_4$/LDH/FTO was not significantly influenced after the addition of interferents species up to a 1000-fold excess The tolerance limit was described as the concentration of interfering spices creating an approximately ±5% relative error in the ETO determination. Thus, it is suggested that the prepared bioelectrode displays high selectivity in the ETO detection even in the presence of interfering molecules.

**Table 2.** Effect of interfering species

| species | Tolerable concentration (analyte: interfering ion) |
|---|---|
| Ibuprofen, acetaminophen | 1:100 |
| ascorbic acid (AA), $Fe^{2+}$ | 1:300 |
| uric acid, glucose, citric acid (UA), Methionine, Valine, caffeine | 1:500 |
| $Na^+$, $K^+$, $Ca^{2+}$, $Mg^{2+}$ | 1:1000 |

### 3.7 Testing on real sample

To further evaluate the feasibility of the proposed DNA /GO/$CoFe_2O_4$/LDH/FTO biosensor, direct determination of ETO in human plasma and urine was carried with the DPV technique. The recovery tests were performed by standard additions of ETO to urine and plasma using the proposed method. Before analysis, the samples collected were separated by centrifuges for 30 min at 4000 rpm and the supernatants were diluted 100 times with PBS buffer. Then different concentrations of ETO were spiked to the above pharmaceutical samples and the recovery values were in the range from 97% to 104% the relative standard deviations (RSDs) for determinations were found to be in the range from 2.2% to 3.6%. The recovery results are shown in Table 3. The results obtained for repeatable on each sample were statistically repeated, corroborating that the DNA/GO/$CoFe_2O_4$/LDH/FTO bioelectrode could be applied for the determination of ETO in real samples.

**Table 3**. Determination of ETO in serum sample solution

| sample | $C_{added}$ (µM) | $C_{found}$ (µM) | Recovery (%) | RSD (%) (n=4) |
|---|---|---|---|---|
| urine | 1.0 | 0.97 | 97 | 2.5 |
| | 4.0 | 4.08 | 102 | 3.6 |
| plasma | 1.0 | 1.04 | 104 | 3.4 |
| | 4.0 | 3.96 | 99 | 2.2 |

## 4. Conclusions

In summary, a new graphene oxide-cobalt ferrite-ZnAl layer double hydroxide nanocomposite which was electrophoretically deposited onto FTO coated glass substrate was successfully synthesized. This GO/$CoFe_2O_4$/ZnAl-LDH/FTO electrode provided an excellent substrate for the DNA immobilization through the electrostatic interaction between positively charged CS ($NH_3^+$)

and negatively charged phosphate ($PO_4^-$) backbone of DNA to fabricate highly sensitive electrochemical DNA biosensor for etoposide (ETO) detection as one of the widely utilized drugs for the treatment of different types of cancers in a wide concentration range (0.2-10 µM). The morphological studies of theDNA/GO/$CoFe_2O_4$/ZnAl-LD/FTO using SEM, EDX and AFM techniques clearly confirmed that the DNA molecules were well immobilized on the surface nanocomposite. The DNA/GO/$CoFe_2O_4$/ZnAl-LDH/FTO bioelectrode showed an increase of electrocatalytic activity in comparison with the pristine LDH and $CoFe_2O_4$/LDH electrode for the ETO detection. The electrochemical results of the fabricated DNA/GO/$CoFe_2O_4$/ZnAl-LD/FTO bioelectrode exhibited a high sensitivity (63.408 µA/µM) and a low detection limit of 0.0010 µM. In addition, this bioelectrode revealed such advantages as easy preparation, long-term stability (6-7 weeks) with 5% loss, excellent selectivity and good reproducibility to etoposide making it a convenient platform for the determination of etoposide in real samples (i. e. plasma and urine) with a recovery range of 97.0%–104.0%. These properties might be assigned to the excellent electron transfer ability, sufficient active sites, good electronic conductivity and high surface area of the nanocomposites, suggesting that they can be an efficient candidate for the other practical applications such as drug delivery systems and cell/enzyme immobilization.

**Acknowledgements**

The authors are grateful to the University of Kashan. Iran for supporting this work by Grant no. (159183/42).

**References**

[1] Y.C. Song, D. Song, W. Feng, X. Shi, H. Li, H.M. Ma, Parallel comparative studies on the toxic effects of unmodified CdTe quantum dots, gold nanoparticles, and carbon nanodots on live cells as well as green gram sprouts, Talanta. 116 (2013) 237-244.

[2] Z. Heger, A. Moulick, V.H. Nguyen, M. Kremplova, P. Kopel, D. Hynek, T. Eckschlager, M. Stiborova, O. Zitka, V. Adam, R. Kizek, Characterization of Multi-Walled Carbon Nanotubes Double-Functionalization with Cytostatic Drug Etoposide and Phosphorothioate Oligodeoxynucleotides. Int. J. Electrochem. Sci. 10 (2015) 7707-7719.

[3] A. E. Radi, N. Abd-Elghany, T. Wahdan, Electrochemical study of the antineoplastic agent etoposide at carbon paste electrode and its determination in spiked human serum by differential pulse voltammetry. Chem. Pharm. Bull. 55 (2007) 1379–1382.

[4] Y.L. Cao, X.L. Du, Z, Zhu, Q. Fu, HPLC Assay for Determination of Etoposide in Human Plasma. Chin. Pharm. J 46 (2011) 857–859.

[5] M. Munawar Hayat, M. Ashraf, N.U. Rehman, F.U.H. Nasım, I. Ahmad, J. Rahman, M. Saleem, M.Z. Malik, HPLC determination of Etoposide in injectable dosage forms. J. Chil. Chem. Soc 56 (2011) 881-883.

[6] J. Tuerk, T.K. Kiffmeyera, C. Hadtsteinc, A. Heinemannd, M. Hahne, H. Stuetzere, H.M. Kussb, U. Eickmann, Development and validation of an LC–MS/MS procedure for environmental monitoring of eight cytostatic drugs in pharmacies. Intern. J. Environ. Anal. Chem. 91 (2011) 1178–1190.

[7] V.L. Demperio, Determination of etoposide phosphate intermediates by gradient liquid chromatography using postcolumn derivatization with cuprammonium hydroxide. J. Chromatogr. A 952 (2002) 283–287.

[8] S.K. Arya, S. Saha, J.E. Ramirez-Vick, V. Gupta, S. Bhansali, S.P. Singh, Recent advances in ZnO nanostructures and thin films for biosensor applications: review. Anal. Chim. Acta. 737 (2012) 737, 1–21. [9] Ji, Q. Ariga, J. P. Hill, Y. Bando, M. Aono, forming nanomaterials as layered functional structures toward materials nanoarchitectonics. NPG. Asia. Mater. 4 (2012) e17.

[10] Y. Wang, H.Y. Xiong, X.H. Zhang, S.F. Wang, Detection of rutin at DNA modified carbon paste electrode based on a mixture of ionic liquid and paraffin oil as a binder. Microchim. Acta. 170 (2010) 27–32.

[11] Ch.L. Bian, Q.X. Zeng, L.J. Yang, H.Y. Xiong, X.H. Zhang, Sh.F. Wang, Voltammetric studies of the interaction of rutin with DNA and its analytical applications on the MWNTs–COOH/Fe3O4 modified electrode. Sens Actuators B Chem 156 (2011) 615– 620.

[12] D.K. Zeybek, B. Demir, B. Zeybek, S. Pekyardımc, A sensitive electrochemical DNA biosensor for antineoplastic drug 5-fluorouracil based on glassy carbon electrode modified with poly (bromocresol purple). Talanta 144 (2015) 793–800.

[13] S. Agarwal, D.K. Jangir, R. Mehrotra, Spectroscopic studies of the effects of anticancer drug mitoxantrone interaction with calf-thymus DNA. J. Photochem. Photobiol. B: Biol 120 (2013) 177–182

[14] M. Muti, M. Muti, lectrochemical monitoring of the interaction between anticancer drug and DNA in the presence of antioxidant. Talanta 178 (2018) 1033–1039.

[15] C. Tserkezidou, A.G. Hatzidimitriou, G. Psomas, Nickel(II) complexes of flufenamic acid: Characterization, structure and interaction with DNA and albumins. Polyhedron 117 (2016) 184–192.

[16] X. Tian, Y.H. Song, H.M. Dong, B.X. Ye, Interaction of anticancer herbal drug berberine with DNA immobilized on the glassy carbon electrode. Bioelectrochemistry. 73 (2008) 18–22.

[17] C. V. Uliana, G. S. Garbellini, H. Yamanaka, Evaluation of the interactions of DNA with the textile dyes Disperse Orange 1 and Disperse Red 1 and their electrolysis products using an electrochemical biosensor, Sensors Actuators B Chem. 178 (2013) 627–635.

[18] Y. Guo, J. Chen, G. Chen, A label-free electrochemical biosensor for detection of HIV related gene based on interaction between DNA and protein. Sens. Actuators B. 184 (2013) 113-117.

[19] A.A. Ensafi, M. Taei, H.R. Rahmani, T. Khayamian, Sensitive DNA impedance biosensor for detection of cancer, chronic lymphocytic leukemia, based on gold nanoparticles/gold modified electrode. Electrochim. Acta. 56 (2011) 8176–8183.

[20] E.L.S. Wong, J.J. Gooding, Charge Transfer through DNA: A Selective Electrochemical DNA Biosensor. Anal. Chem. 78 (2006) 2138.

[21] P.R. Solanki, A. Kaushik, V.V. Agrawal, Malhotra, B.D. Nanostructured metal oxide-based biosensors. NPG Asia Mater. 3 (2011) 7–24.

[22] M.I. Pividori, A. Merkoci, S. Alegret, Electrochemical genosensor design: immobilization of oligonucleotides onto transducer surfaces and detection methods. Biosens. Bioelectron. 15 (2000) 291–303.

[23] X. Zhao, F. Pan, P. Coffey, J.R. Lu, Cationic copolymer–mediated DNA immobilization: interfacial structure and composition as determined by ellipsometry, dual polarization interferometry, and neutron reflection. Langmuir. 2 (2008) 13556–13564.

[24] L. Li-Ping, W. Shu-Qing, L. Xiang-Qin, Fabrication of layer-by-layer deposited multilayer films containing DNA and gold nanoparticle for norepinephrine biosensor. Anal. Chim. Acta. 519 (2004) 161–166.

[25] A. Mehdinia, S. Habib, S. Kazemi, Z. Bathaie, A. Alizadeh, Mo. Shamsipur, M.F. Mousavi, Electrochemical studies of DNA immobilization onto the azide-terminated monolayers and its interaction with taxol, Anal. Biochem. 375 (2008) 331–338.

[26] H. Bhardwaj, Sh. Solanki, G. Sumana, Electrophoretically deposited multiwalled carbon nanotube based amperometric genosensor for E. coli detection. J. Phys. Conf. Ser. 704 (2016) 012007.

[27] P. Arias, N. F. Ferreyra, G.A. Rivas, S. Bollo, Glassy carbon electrodes modifies with CNT dispersed in chitosan: analytical applications for sensing DNA–methylene blue interaction. J. Electroanal. Chem. 634 (2009) 123–126.

[28] R. Singha, R. Verma, A. Kaushik, G. Sumana, S. Sood, R.K. Gupta, B.D. Malhotra, Chitosan–iron oxide nano-composite platform for mismatch-discriminating DNA hybridization for Neisseria gonorrhoeae detection causing sexually transmitted disease. Biosens. Bioelectron. 26 (2011) 2967–2974.

[29] A.E. Radi, H.M. Nassef, A. Eissa, Voltammetric and ultraviolet-visible spectroscopic studies on the interaction of etoposide with deoxyribonucleic acid. Electrochim. Acta. 113 (2013) 164-169.

[30] J. Yuan, SH. Xu, H.Y. Zeng, X. Cao, A.D. Pan, G.F. Xiao, P.X. Ding, Hydrogen peroxide biosensor based on chitosan/2D layered double hydroxide composite for the determination of $H_2O_2$, Bioelectrochemistry. 123 (2018**)** 94–102.

[31] Y. Dou, S. Zhang, T. Pan, S. Xu, A. Zhou, M. Pu, H. Yan, J. Han, M. Wei, D.G. Evans, X. Duan, $TiO_2$@Layered double hydroxide core-shell nanospheres with largely enhanced photocatalytic activity toward $O_2$ generation. Adv. Funct. Mater. 25 (2015) 2243-2249.

[32] Z. Bouaziz, L. Soussan, J.M. Janot, M. Jaber, A.B.H. Amara, S. Balme, Dual role of layered double hydroxide nanocomposites on antibacterial activity and degradation of tetracycline and oxytetracyline, Chemosphere. 206 (2018) 175-183.

[33] X. Li, J. Liu, X. Ji, J. Jiang, R. Ding, Y. Hu, A. Hu, X. Huang. Ni/Al layered double hydroxide nanosheet film grown directly on Ti substrate and its application for a nonenzymatic glucose sensor. Sens. Actuators. B 147 (2010) 241–247.

[34] H. Zhang, R. Qi, D.G. Evans, X. Duan, Synthesis and characterization of a novel nano-scale magnetic solid base catalyst involvinga layered double hydroxide supported on a ferrite core. J. Solid State Chem. 177 (2004) 772-780.

[35] K. Vijaya Sankar, R. Kalai Selvan, D. Meyrick, Electrochemical performances of $CoFe_2O_4$ nanoparticles and a rGO based asymmetric supercapacitor. RSC Adv. 5 (2015) 99959-99967.

[36] Z. Yang, Y. Zhu, M. Chi, C. Wang, Y. Wei, X. Lu, Fabrication of cobalt ferrite/cobalt sulfide hybrid nanotubes with enhanced peroxidase-like activity for colorimetric detection of dopamine, J. Colloid. Interface. Sci. 511 (2018) 383-391.

[37] G. Wang, F. Zhou, X. Li, J. Li, Y. Ma, J. Mu, Z. Zhang, H. Che, X. Zhang, Controlled synthesis of L-cysteine coated cobalt ferrite nanoparticles for drug delivery. Ceram. Int. 44 (2018) 13588-13594.

[38] B. Thomas, L.K. Alexander, Enhanced synergetic effect of Cr(VI) ion removal and anionic dye degradation with superparamagnetic cobalt ferrite meso–macroporous nanospheres. Appl. Nanosci. 8 (2018) 125-135.

[39] Z. Shahnavaz, P.M. Woi, Y. Alias, A hydrothermally prepared reduced graphene oxide-supported copper ferrite hybrid for glucose sensing. Ceram. Int. 4 (2015) 12710–12716.

[40] F.S. Vajedi, H. Dehghani, Synthesis of titanium dioxide nanostructures by solvothermal method and their application in preparation of nanocomposite based on graphene. J. Mater. Sci. 51 (2015) 1845-1854.

[41] F.S. Vajedi, H. Dehghani, The characterization of $TiO_2$-reduced graphene oxide nanocomposites and their performance in electrochemical determination for removing heavy metals ions of cadmium(II), lead(II) and copper(II). Mater. Sci. Eng. B. 243 (2019) 189-198.

[42] L. Mao, K. Ji, L. Yao, X. Xue, W. Wen, X. Zhang, Sh. Wang, Molecularly imprinted photoelectrochemical sensor for fumonisin B1 based on GO-CdS heterojunction. Biosensors and Bioelectronics. 127 (2019) 57-63.

[43] X. L. Wu, L. Wang, C.L. Chen, A.W. Xu, X.K. Wang, Water-Dispersible Magnetite-Graphene-LDH Composites for Efficient Arsenate Removal. J. Mater. Chem. 21 (2011) 17353−17359.

[44] F. Zhang, Y. Song, SH. Song, R. Zhang, W. Hou, Synthesis of Magnetite−Graphene Oxide-Layered Double Hydroxide Composites and Applications for the Removal of Pb(II) and 2,4- Dichlorophenoxyacetic Acid from Aqueous Solutions. ACS Appl. Mater. Interfaces. 7 (2015) 7251–7263.

[45] B. Bozal-Palabiyik, B. Dogan-Topal, B. Uslu, A. Can, S.A. Ozkan, Sensitive voltammetric assay of etoposide using modified glassy carbon electrode with a dispersion of multi-walled carbon nanotube, J. Solid State Electrochem. 17 (2013) 2815–2822.

[46] I. Tzouvadaki, N.A. akbarinodehi, D. D´avila, G. De Micheli, S. Carrara, Graphene Nanowalls for High-Performance Chemotherapeutic Drug Sensing and Anti-Fouling Properties. Sens. Actuators. B. 262 (2018) 395-403.

[47] J. Song, Q. Chen, Y. Zhang, M. Diba, E. Kolwijck, J. Shao, J. A. Jansen, F. Yang, A. R. Boccaccini, S. C. G. Leeuwenburgh, Electrophoretic Deposition of Chitosan Coatings Modified with Gelatin Nanospheres to Tune the Release of Antibiotics ACS Appl. Mater. Interfaces, 8 (2016), 13785–13792.

[48] M.E. Reichmann, C.A. Rice, C.A. Thomas, P, Doty, A Further Examination of the Molecular Weight and Size of Desoxypentose Nucleic Acid. J. Am. Chem. Soc. 76 (1954) 3047-3053.

[49] W. Hummers, R. Offeman, Preparation of Graphitic Oxide. J. Am. Chem. Soc, 1958, 80, 1339–1340.

[50] W. Yu, H. Xianwei, L. He, L. Guo. A Sensitive impedimetric DNA biosensor based on (Nb,V) codoped $TiO_2$ for breast cancer susceptible gene detection. Mater. Sci. Eng. C. 77 (2017) 867–873.

[51] M.Y. Nassar, M. Khatab, Cobalt ferrite nanoparticles via a template-free hydrothermal route as an efficient nano-adsorbent for potential textile dye removal. RSC Adv. 6 (2016) 79688-79705.

[52] Q. Gong, H. Yang, Y. Dong and W. Zhang, A sensitive impedimetric DNA biosensor for the determination of the HIV gene based on electrochemically reduced graphene oxide, Anal. Methods, 7 (2015) 2554-2562,

[53] Q. Zhuang, J. Chen, J. Chen, X. Lin, Electrocatalytical properties of bergenin on a multi-wall carbon nanotubes modified carbon paste electrode and its determination in tablets. Sens. Actuators. B: Chem. 128 (2008) 500–506.

[54] H.V. Nguyen, L. Richtera, A. Moulick, K. Xhaxhiu, J. Kudr, N. Cernei, H. Polanska, Z. Heger, M. Masarik, P. Kopel, Electrochemical sensing of etoposide using carbon quantum dot modified glassy carbon electrode. Analyst. 141 (2016) 2665–2675.

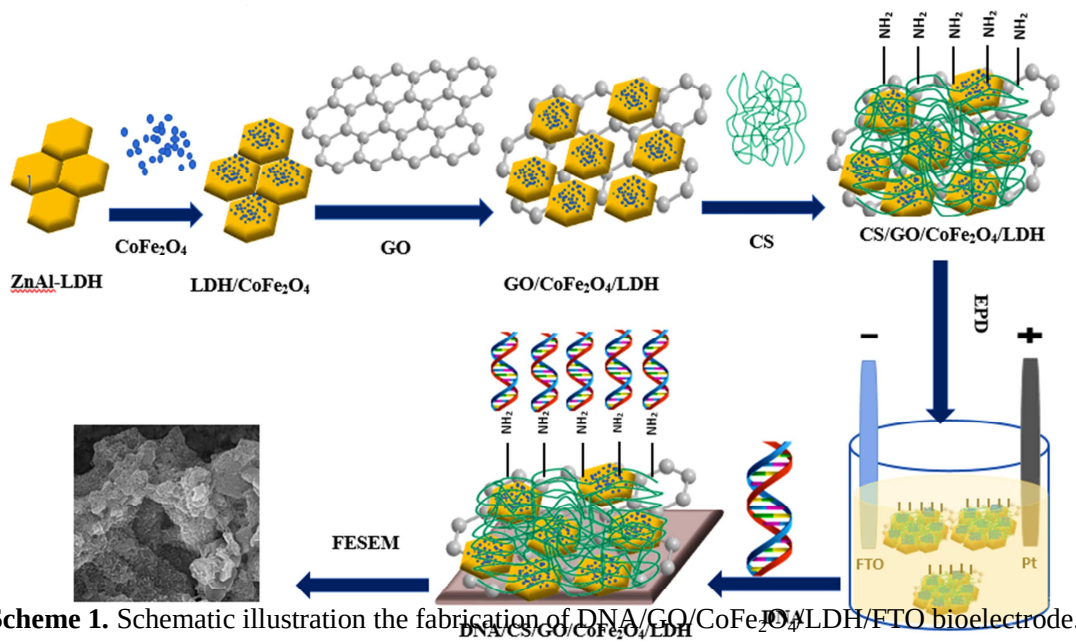


**Scheme 1.** Schematic illustration the fabrication of DNA/GO/$CoFe_2O_4$/LDH/FTO bioelectrode.

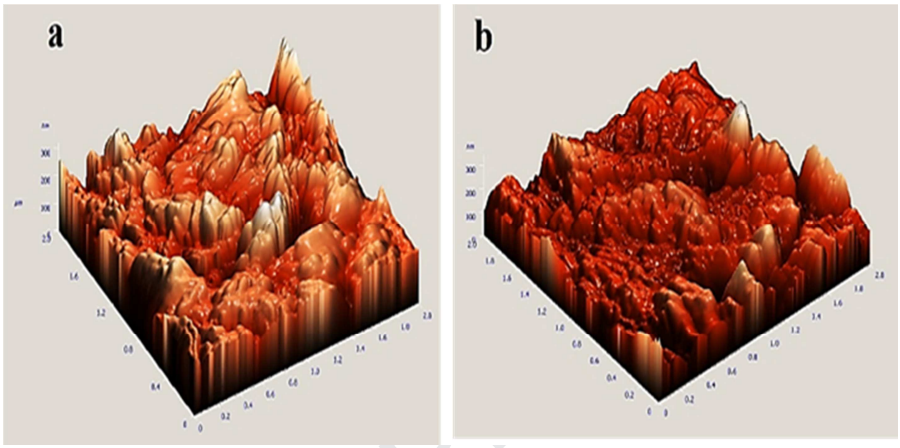


**Fig. 1** 3-Dimensional (3D) AFM images of the (a) GO/$CoFe_2O_4$/LDH and (b) DNA/GO/$CoFe_2O_4$/LDH thin films on the FTO.

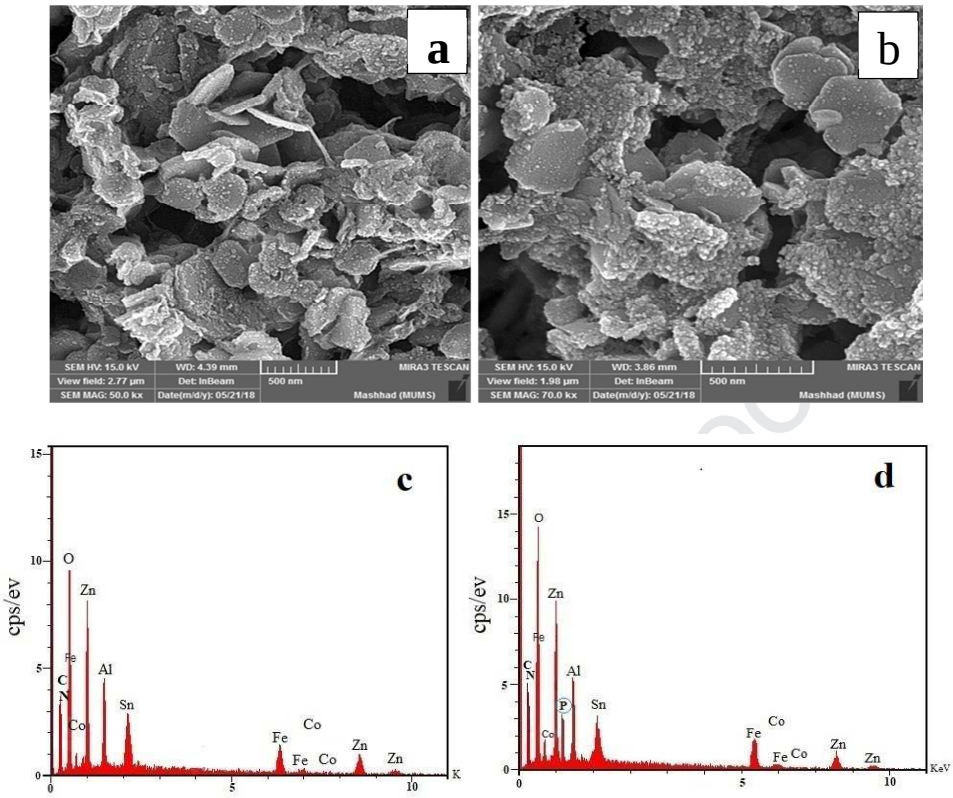


**Fig. 2** FESEM images of (a) GO/$CoFe_2O_4$/ZnAl-LDH and (b) DNA/GO/$CoFe_2O_4$/ZnAl-LDH thin films on the FTO; (c) EDX of GO/$CoFe_2O_4$/ZnAl-LDH and (d) DNA/GO/$CoFe_2O_4$/ZnAl-LDH.

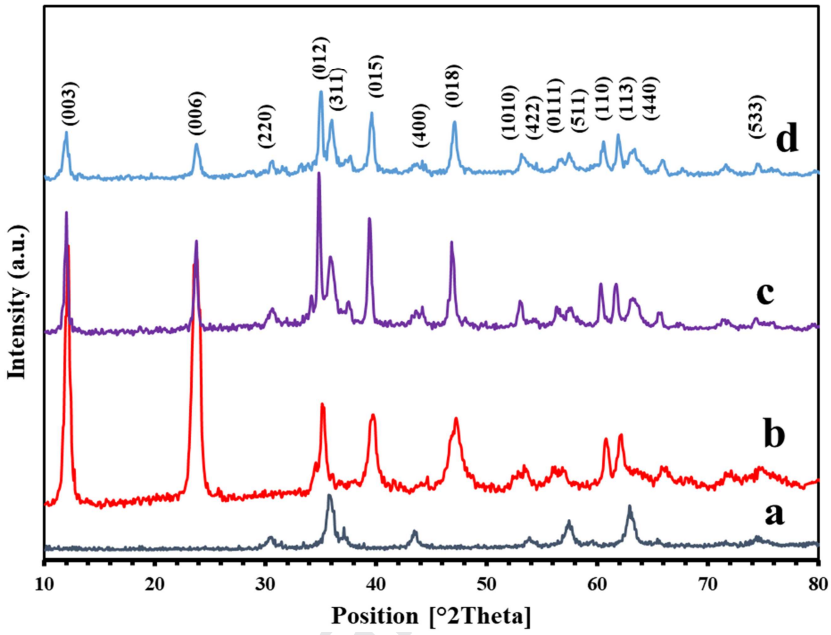


**Fig. 3** XRD patterns of $CoFe_2O_4$ (a), LDH (b), $CoFe_2O_4$/ZnAl-LDH (c) and GO/$CoFe_2O_4$/ZnAl-LDH (d) (e) nanocomposites.

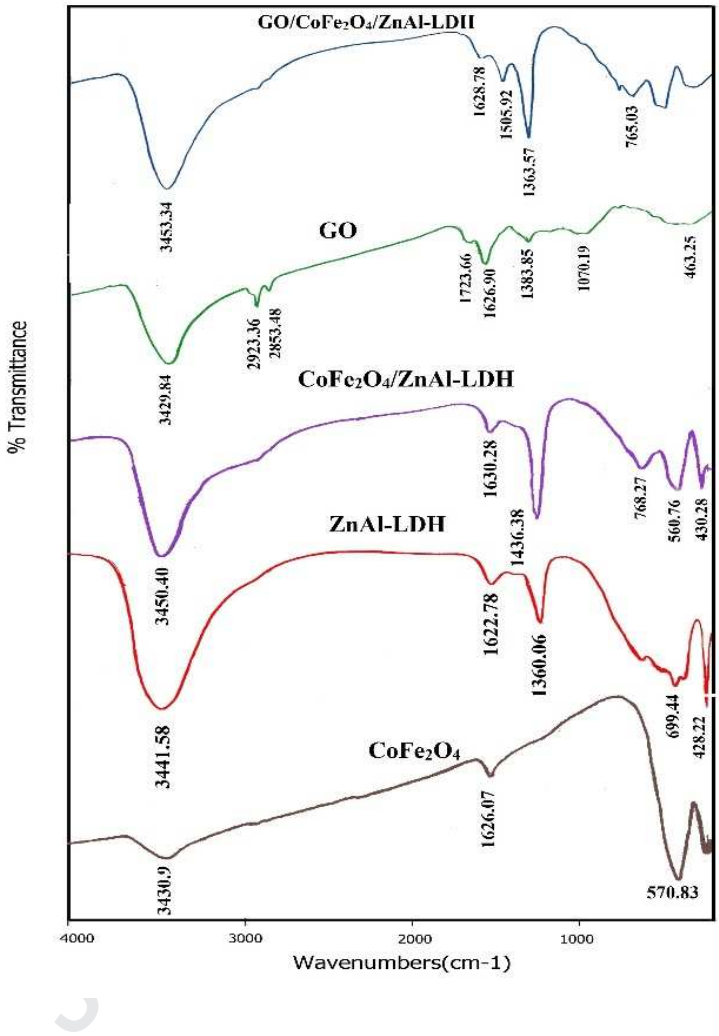


**Fig. 4** FT-IR spectra of $CoFe_2O_4$, ZnAl-LDH, $CoFe_2O_4$/ZnAl-LDH, GO and GO/$CoFe_2O_4$/ZnAl-LDH samples.

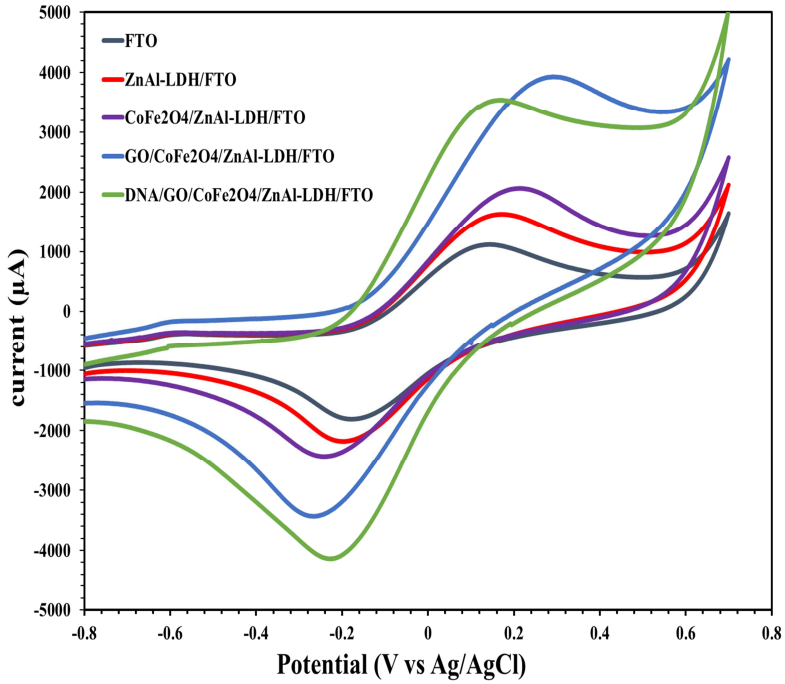


**Fig. 5** Cyclic voltammograms of various electrodes in PBS (20 mM, pH 7.4, 0.9% NaCl) containing $[Fe(CN)6]^{3-/4-}$ (5 mM)] at 100 mV $s^{-1}$.

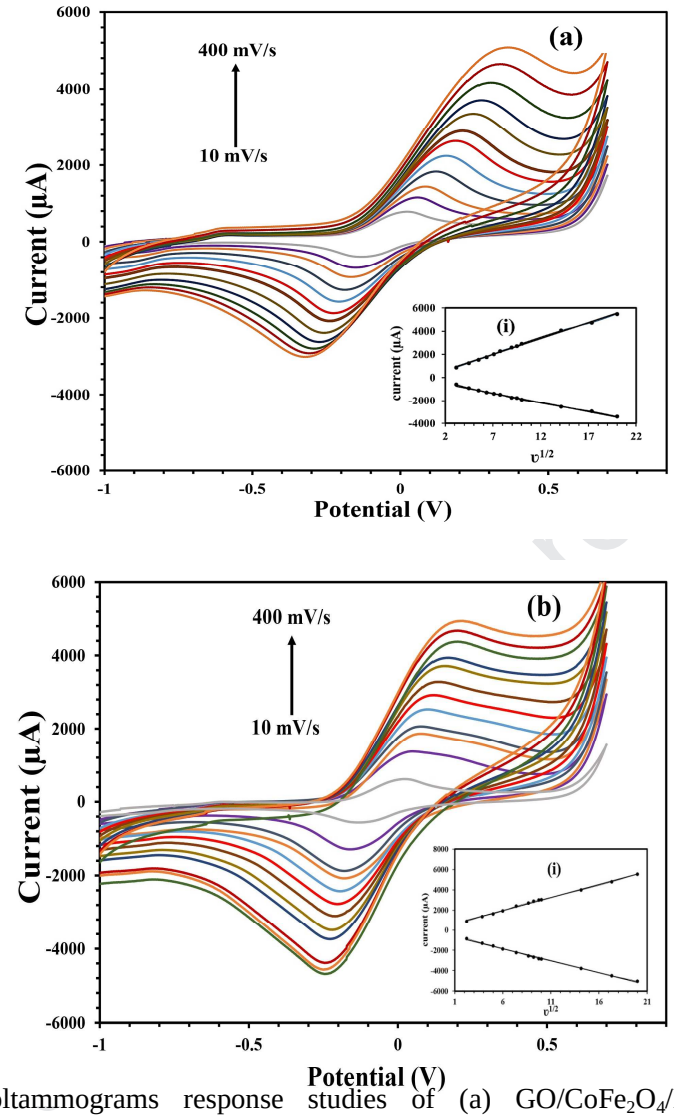


**Fig. 6** Cyclic voltammograms response studies of (a) GO/$CoFe_2O_4$/LDH/FTO electrode (b) DNA/GO/$CoFe_2O_4$/LDH/FTO bioelectrode as a function of scan rate (10 to 400 mV/s) (inset: shows the variation of (i) current with square root of scan rate and (ii) potential with log of scan rate).

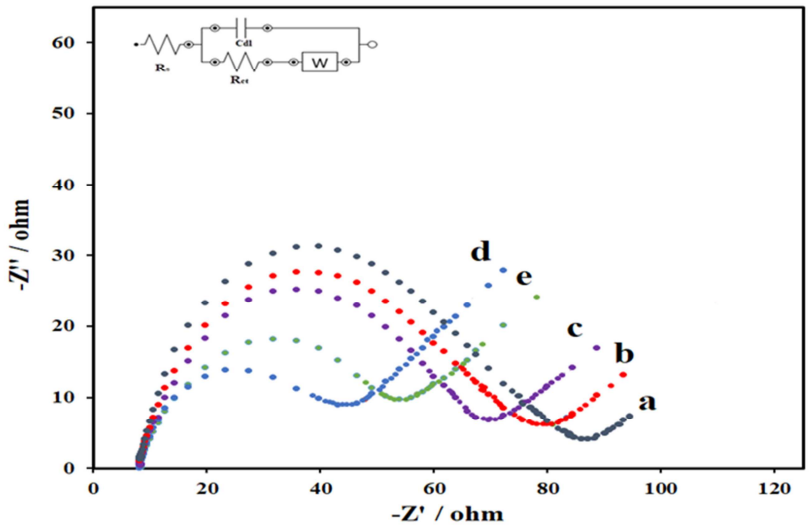


**Fig. 7** EIS curves of (a) FTO, (b) LDH/FTO (c) $CoFe_2O_4$/LDH/FTO electrode (d) DNA/GO/$CoFe_2O_4$/LDH/FTO electrode and (e) GO/$CoFe_2O_4$/LDH/FTO bioelectrode in PBS solution (pH 7.4) containing 5 mM $[Fe(CN)_6]^{3-/4-}$: Inset: Randle's circuit.

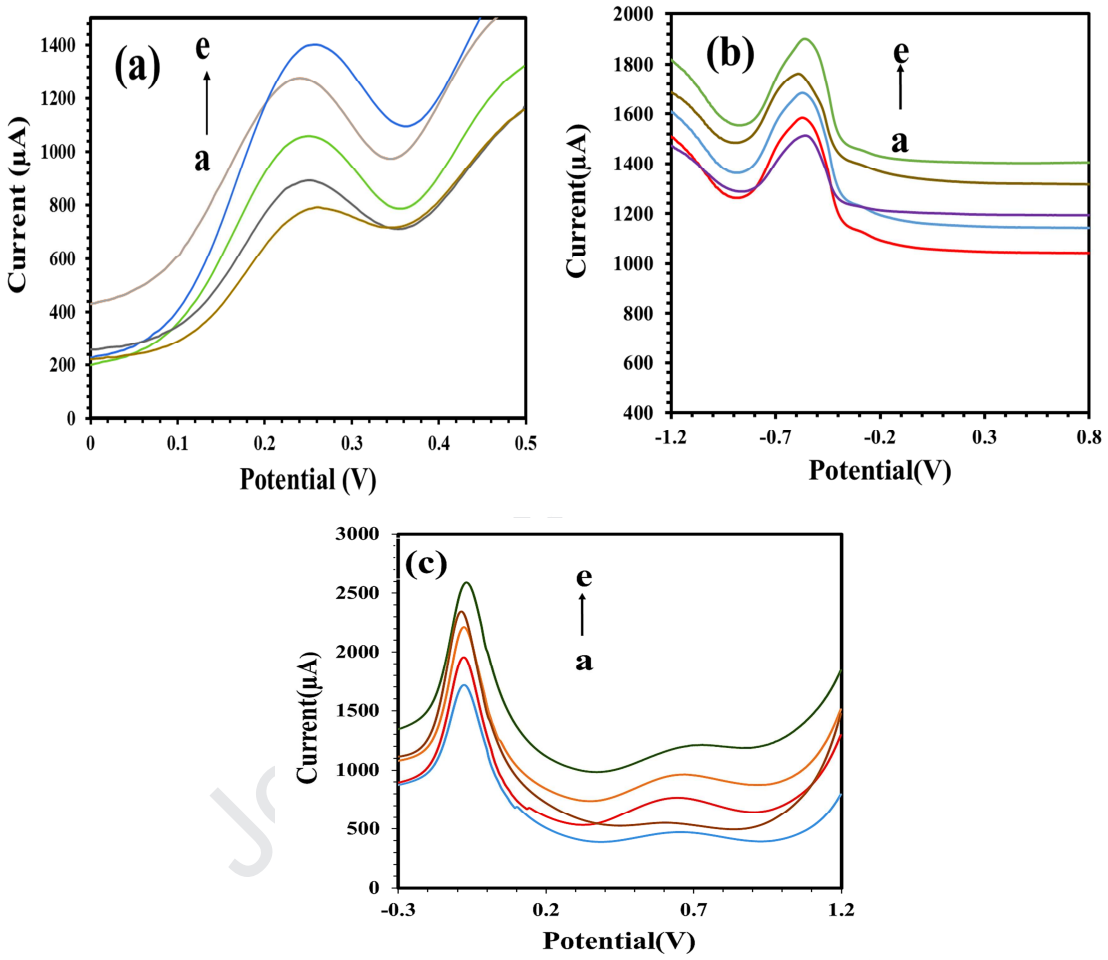


**Fig. 8** DPV response (a) and SWASV (b, c) of bare FTO (Curve a), LDH/FTO (Curve b), $CoFe_2O_4$/LDH/FTO (Curve c), DNA/GO/$CoFe_2O_4$/LDH/FTO bioelectrode (Curve d) and GO/$CoFe_2O_4$/LDH/FTO (Curve e) in the absence (a), presence ETO in phosphate buffer of pH 7.4 (b) and PBS solution containing 5mM[Fe(CN)6]3−/4− (c), respectively.

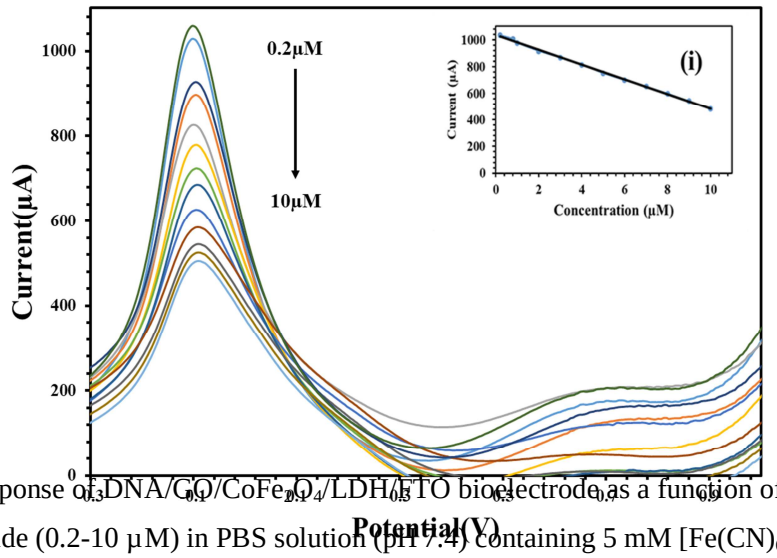


**Fig. 9** DPV response of DNA/GO/$CoFe_2O_4$/LDH/FTO bioelectrode as a function of different concentrations of etoposide (0.2-10 µM) in PBS solution (pH 7.4) containing 5 mM $[Fe(CN)_6]^{3-/4-}$. (inset shows a linear plot of the DPV response of DNA/GO/$CoFe_2O_4$/LDH/FTO bioelectrode as a function of concentration of etoposide.

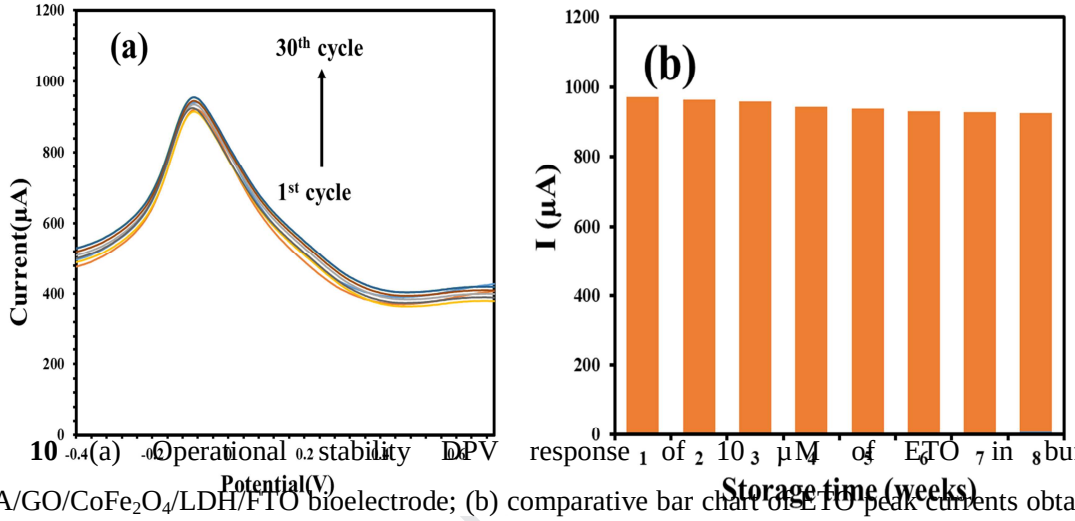


**Fig. 10** (a) Operational stability DPV response of 10 µM of ETO in buffer at DNA/GO/$CoFe_2O_4$/LDH/FTO bioelectrode; (b) comparative bar chart of ETO peak currents obtained for eight weeks using Au- DNA/GO/$CoFe_2O_4$/LDH/FTO bioelectrode at 10 µM of ETO in buffer.

**Highlights**

- A novel DNA biosensor was constructed electrophoretically based on graphene oxide-cobalt ferrite-ZnAl/layered double hydroxide composite and utilized for the electrochemical detection of ETO.
- CV, EIS and DPV were employed to investigate the electrochemical characterization of the GO/$CoFe_2O_4$/LDH/FTO.
- The developed biosensor demonstrated ultrasensitivity in detection of etoposide with low detection limit of 0.0010 µM for ETO.
- Develop bioelectrode was successfully used to quantify etoposide in real human samples with recovery from 97.0% to 104.0%.